

# We are IntechOpen, the world's leading publisher of Open Access books Built by scientists, for scientists

4,800

Open access books available

122,000

International authors and editors

135M

Downloads

Our authors are among the

154

Countries delivered to

TOP 1%

most cited scientists

12.2%

Contributors from top 500 universities



WEB OF SCIENCE™

Selection of our books indexed in the Book Citation Index  
in Web of Science™ Core Collection (BKCI)

Interested in publishing with us?  
Contact [book.department@intechopen.com](mailto:book.department@intechopen.com)

Numbers displayed above are based on latest data collected.  
For more information visit [www.intechopen.com](http://www.intechopen.com)



# Van der Waals and Graphene-Like Layers of Silicon Nitride and Aluminum Nitride

Vladimir G. Mansurov, Yuriy G. Galitsyn, Timur V. Malin, Sergey A. Teys, Konstantin S. Zhuravlev, Ildiko Cora and Bela Pecz

## Abstract

A systematic study of kinetics and thermodynamics of Si (111) surface nitridation under ammonia exposure is presented. The appeared silicon nitride ( $8 \times 8$ ) structure is found to be a metastable phase. Experimental evidences of graphene-like nature of the silicon nitride ( $8 \times 8$ ) structure are presented. Interlayer spacings in the  $(\text{SiN})_2(\text{AlN})_4$  structure on the Si (111) surface are found equal to 3.3 Å in SiN and 2.86 Å in AlN. These interlayer spacings correspond to weak van der Waals interaction between layers. In contrast to the widely accepted model of a surface structure ( $8 \times 8$ ) as monolayer of  $\beta\text{-Si}_3\text{N}_4$  on Si (111) surface, we propose a new graphene-like  $\text{Si}_3\text{N}_4$  (g- $\text{Si}_3\text{N}_3$  and/or g- $\text{Si}_3\text{N}_4$ ) model for the ( $8 \times 8$ ) structure. It is revealed that the deposition of Al atoms on top of a highly ordered ( $8 \times 8$ ) structure results in graphene-like AlN (g-AlN) layers formation. The g-AlN lattice constant of 3.08 Å is found in a good agreement with the *ab initio* calculations. A transformation of the g-AlN to the bulk-like wurtzite AlN is analyzed.

**Keywords:** kinetics and thermodynamics of 2D layers formation, van der Waals interaction, graphene-like silicon nitride, g-AlN,  $\text{sp}^3$ - and  $\text{sp}^2$ -hybridization,  $\pi$ -orbitals, RHEED, STM, STS, HRTEM

## 1. Introduction

After the discovery of graphene, significant effort is spent to create other graphene-like (graphite-like) materials. Among them, much attention was attracted to graphite-like carbon-nitride compounds g- $\text{C}_3\text{N}_3$  and g- $\text{C}_3\text{N}_4$  [1–10]. These materials consist of covalently bound  $\text{sp}^2$ -hybridized carbon and nitrogen atoms. Interest in them is caused by theoretical predictions of new mechanical, electronic, magnetic, and photocatalytic properties [1–9]. To date, the compound g- $\text{C}_3\text{N}_4$  has been synthesized [10], and it has been demonstrated that the layers of g- $\text{C}_3\text{N}_4$  have a bandgap width in the range of 1.6–2.0 eV, which makes it possible to use the semiconductor layer to create electronics and optoelectronics devices, such as field effect transistors, photodetectors, light-emitting diodes, and lasers. Since silicon is in the same group as carbon in the periodic table, then graphene-like Si-N sheets, where C atoms are replaced by Si atoms, are expected to demonstrate the unusual properties.

Dielectric materials that provide insulation of conductive channels are also necessary for the development of electronic devices. Hexagonal-BN (h-BN), one of the 2D dielectric materials [11, 12], attracts grate attention. However, the fabrication of large area h-BN layers is difficult. AlN is another alternative dielectric material that can be grown epitaxially on large areas. It is also predicted [13] that silicene is stable when encapsulating between two thin graphite-like hexagonal AlN layers. This is especially important, since until now silicene growth has been presented only on metal substrates, which makes it unsuitable for electronic devices. In this chapter, the synthesis and properties of the graphene-like materials and van der Waals layers of silicon nitride (g-SiN) and aluminum nitride (g-AlN) are reported.

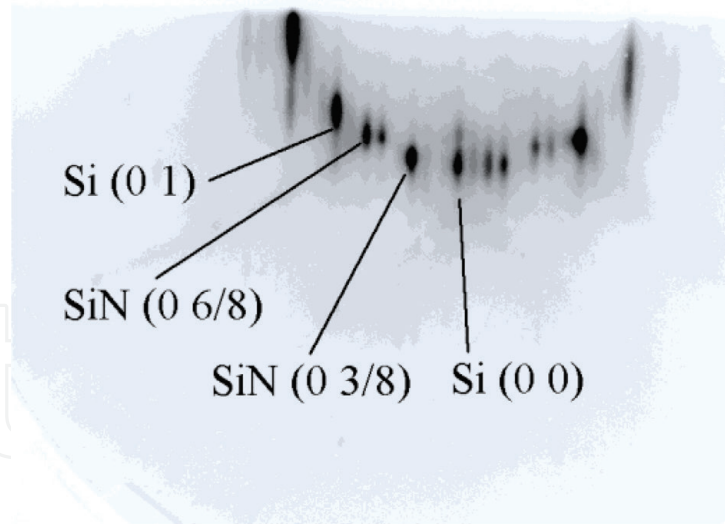
## 2. Kinetics and thermodynamics of g-SiN formation on the Si (111) surface

### 2.1 Formation kinetics of silicon nitride

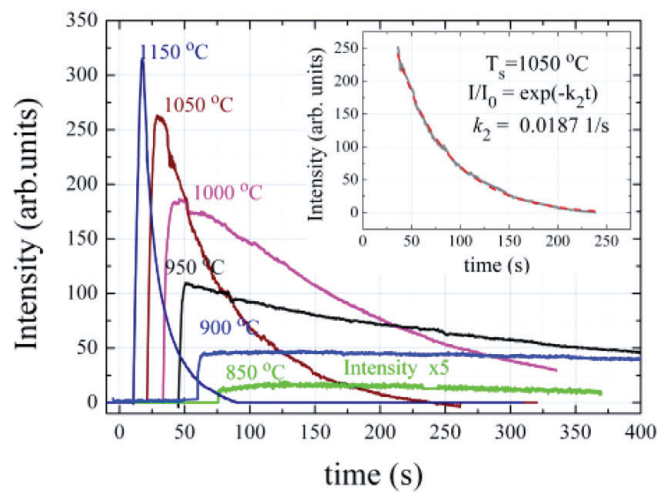
The  $\text{Si}_3\text{N}_4$  film formed on the silicon surface as a rule is amorphous [14–18]. However, at the initial stage of this process, the  $(8 \times 8)$  structure is formed. The structure  $(8 \times 8)$  was first discovered by van Bommel and Meyer in 1967 [19]. This structure has been actively studied later. “Modifications” of this structure such as  $(11/8 \times 11/8)$  and  $(3/8 \times 3/8)$  have been discovered and described. Models explaining the appearance of  $(8 \times 8)$  structure by forming a layer of crystalline silicon nitride  $\beta\text{-Si}_3\text{N}_4$  are dominating in the literature [20–24].

In our experiments, the nitridation of the silicon surface is started by the onset of ammonia flux onto the clean Si (111) substrate heated to temperatures above  $750^\circ\text{C}$  [25]. Two different stages of the silicon nitridation were distinguished by reflection high energy electron diffraction (RHEED): the first stage is a fast formation of the  $(8 \times 8)$  structure and the following stage is a slow formation of amorphous  $\text{Si}_3\text{N}_4$  phase. The ordered  $(8 \times 8)$  structure appears within a few seconds under ammonia flux for the all used temperatures. RHEED pattern of  $(8 \times 8)$  obtained after exposure of the surface during 6 s under ammonia flux  $F_{\text{NH}_3} = 10$  sccm at a temperature  $T = 1050^\circ\text{C}$  is shown in **Figure 1a**. The following bright diffraction spots corresponding to the  $(8 \times 8)$  structure are clearly observed (**Figure 1a**):  $(0 -3/8)$ ,  $(0 -5/8)$ ,  $(0 -6/8)$ ,  $(0 -11/8)$ , as well as weaker reflections of  $(0 -1/8)$ ,  $(0 -2/8)$ , and  $(0 -7/8)$  along with the fundamental reflexes  $(0 0)$ ,  $(0 1)$ , and  $(0 1)$  of the Si (111) surface. However, the diffraction spots such as  $(0 \pm 4/8)$  or  $(\pm 4/8 \pm 4/8)$  related to the fundamental periodicity of the crystalline phase of  $\beta\text{-Si}_3\text{N}_4$  were not observed. This experimental fact indicates that the structure  $(8 \times 8)$  does not correspond to the  $\beta\text{-Si}_3\text{N}_4$  phase, in contrast to the dominating interpretation of nature of the structure  $(8 \times 8)$  [20–24].

Further nitridation at the same conditions (the second stage) results in silicon nitride amorphous phase ( $\alpha\text{-Si}_3\text{N}_4$ ) formation that was accompanied by the total disappearance of all diffraction spots in the RHEED pattern within several minutes. The behavior of intensities of the fractional  $(0 3/8)$  diffraction spot as a function of time (i.e., kinetic curves) at different substrate temperatures is shown in **Figure 1b**. **Figure 1b** clearly demonstrates the fast rise of the fractional  $(0 3/8)$  spot intensity (the first fast stage) and its further decay of the diffraction spot (the second slow stage). The thickness of  $\alpha\text{-Si}_3\text{N}_4$  in our experiments was about 5–30 Å, depending on the duration of nitridation. These data do not confirm the possibility of epitaxial growth of crystalline  $\beta\text{-Si}_3\text{N}_4$  layers, as was supposed in works [22, 23]. We revealed that the diffraction spot intensity decay as function of time is well described by the exponential law  $I(t) = I_0(T) \times \exp(-k_2(T) \cdot t)$  at all investigated temperatures T,



(a)



(b)

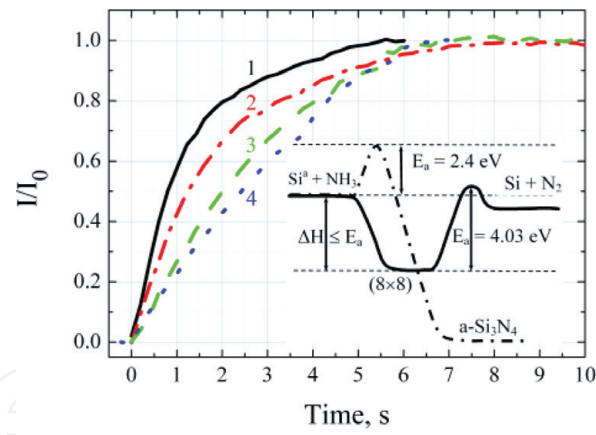
**Figure 1.**

(a) RHEED pattern of the structure ( $8 \times 8$ ) appeared on the Si ( $111$ ) substrate after its exposure to 10 sccm ammonia flux for 6 s at temperature of  $1050^\circ\text{C}$ ; (b) the behavior of fractional ( $0\ 3/8$ ) spot intensities at different substrate temperatures, from [25]. The inset **Figure 1b** shows approximation of the kinetic curve taken at  $T = 1050^\circ\text{C}$  (gray, solid) by the exponential function (red, dash).

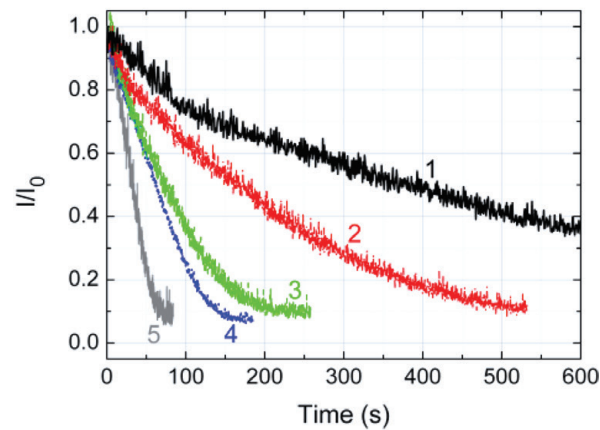
where  $k_2$  is the rate constant and  $t$  denotes time, and so this process corresponds to a first-order reaction. As an example, the inset in **Figure 1b** shows approximation of the experimental curve by the exponential law at  $T = 1050^\circ\text{C}$ . The activation energy of the amorphous silicon nitride phase formation of 2.4 eV and pre-exponential factor of  $10^7$ – $10^8$  1/s is found.

**Figure 2a** shows the normalized kinetic curves for the formation of the ( $8 \times 8$ ) structure, measured by the intensity evolution of the ( $0\ 3/8$ ) spot. The figure clearly shows that there is a slight decrease in the rate of formation of the structure ( $8 \times 8$ ) with increasing temperature, which indicates the absence of an activation barrier in this process in contrast to a-Si<sub>3</sub>N<sub>4</sub> formation. This fact also does not agree with the formation of a crystalline  $\beta$ -Si<sub>3</sub>N<sub>4</sub> layer, which requires the overcoming of a large activation barrier [26].

As shown in work [25], at the formation of the structure ( $8 \times 8$ ), the main role is played by mobile silicon adatoms (Si<sup>a</sup>), which are in equilibrium with the surface of the silicon crystal at a given temperature, and the heat of the mobile adatoms formation is 1.7 eV. The existence of mobile adatoms is well known, for example, in the



(a)



(b)

**Figure 2.**

(a) Evolution of the intensity of the  $(0\ 3/8)$  spot during the formation of the  $(8 \times 8)$  structure at different temperatures: 1.  $900^\circ\text{C}$ , 2.  $1000^\circ\text{C}$ , 3.  $1050^\circ\text{C}$ , 4.  $1150^\circ\text{C}$ ; (b) kinetic curves of thermal decomposition of the structure  $(8 \times 8)$ : 1.  $980^\circ\text{C}$ , 2.  $1005^\circ\text{C}$ , 3.  $1030^\circ\text{C}$ , 4.  $1040^\circ\text{C}$ , 5.  $1055^\circ\text{C}$ . All curves are normalized to their own maximum intensity. The inset **Figure 2a** demonstrates energy diagrams: the solid curve corresponds to formation and decomposition of the structure  $(8 \times 8)$  and the dashed-dotted curve corresponds to formation of amorphous  $\text{Si}_3\text{N}_4$ .

temperature range of about  $1000^\circ\text{C}$ , and mobile silicon adatoms provide movement of steps on the surface, the formation and/or disappearance of two-dimensional islands, and participate in oxidation processes and other surface reactions [27–29]. Since the rate of formation of the structure  $(8 \times 8)$  is high during the nitridation process, then the equilibrium concentration of mobile adatoms  $\text{Si}^a$  does not have time to be established and the coverage of the surface by the two-dimensional phase  $(8 \times 8)$  is determined by the initial concentration of mobile silicon adatoms at the Si surface at a given temperature. In diffraction, this is manifested in the temperature dependence of the maximum intensity  $I_0(T)$ . It should be emphasized one more time that the formation of the structure  $(8 \times 8)$  originates from interaction of ammonia with the mobile silicon adatoms rather than the dangling bonds of silicon atoms incorporated in lattice site (i.e., immobile) on the Si (111) surface.

## 2.2 Thermal decomposition of a two-dimensional layer $(8 \times 8)$

We investigated the stability of the phase  $(8 \times 8)$  by studying the kinetics of thermal decomposition of the structure  $(8 \times 8)$  under ultrahigh vacuum conditions for the temperature range  $980$ – $1055^\circ\text{C}$  using the RHEED spots intensity evolution. When the sample was held for several minutes at a fixed temperature, the fractional

diffraction spots of the structure ( $8 \times 8$ ) were faded away and the ( $1 \times 1$ ) pattern of the clean silicon surface was restored. **Figure 2b** shows the normalized kinetic curves of the thermal decomposition of the structure ( $8 \times 8$ ) at different temperatures. Analysis of these curves showed that the rate of thermal decomposition increases with increasing temperature, that is, the ( $8 \times 8$ ) structure decomposition is a normal activation process. Curves are well described by a decreasing exponential law  $I(t) = I_0 \exp(-k(T)/t)$ , where  $t$  is the time,  $k$  is the constant of the decomposition rate of the structure ( $8 \times 8$ ), and  $T$  is the surface temperature.

The thermal decomposition constant  $k$  as function of temperature is presented in the Arrhenius coordinates in **Figure 3**. The activation energy ( $E_a$ ) of the structure ( $8 \times 8$ ) thermal decomposition,  $E_a = 4.03$  eV, and the pre-exponential factor,  $k_0 = 2.4 \times 10^{13}$  1/s, are found. The value of  $E_a$  is close to the known binding energy of Si-N bond in  $\text{Si}_3\text{N}_4$ —4.5 eV [30]. Since the activation energy of the decomposition cannot be less than the heat of formation (that is,  $E_a \geq \Delta H$ ), then the heat of formation of the structure ( $8 \times 8$ )  $\Delta H$  is no more than 4 eV. The inset of **Figure 2a** schematically illustrates the relationship between the heat of formation and the activation energy of the thermal decomposition of the structure ( $8 \times 8$ ), as well as it shows the energy diagram of the  $\text{Si}_3\text{N}_4$  amorphous phase formation. The heat of formation of bulk  $\beta$ - $\text{Si}_3\text{N}_4$  is about 8 eV [26, 31], which is much larger than the heat of the ( $8 \times 8$ ) structure formation estimated here.

The decomposition rate of the  $\beta$ - $\text{Si}_3\text{N}_4$  crystalline phase surface, which was studied in the work [31], is much slower in comparison with the decomposition of the structure ( $8 \times 8$ ), for example, at a temperature of  $1740^\circ\text{C}$ , the surface decomposition process took more than an hour. In our case, at a much lower temperature,  $T = 1055^\circ\text{C}$ , the complete decay of the structure ( $8 \times 8$ ) takes about a minute, which confirms the lower thermal stability of the structure ( $8 \times 8$ ) in comparison with the  $\beta$ - $\text{Si}_3\text{N}_4$  crystal. The activation energy of the decomposition of the structure ( $8 \times 8$ ) measured here coincides with the activation energy of the surface thermal decomposition of  $\beta$ - $\text{Si}_3\text{N}_4$  (93 kcal/mol), but the pre-exponential factor ( $2.4 \times 10^{13}$  1/s) is  $10^6$  times higher than the pre-exponential factor of  $\beta$ - $\text{Si}_3\text{N}_4$  surface decomposition ( $10^7$  1/s) [31]. The coincidence of activation energies shows that in both cases, the limiting stage of the processes is the breaking of the Si-N bonds but the rates of the processes differ by a factor of  $10^6$ . We note that the measured pre-exponential factor has a normal value of  $\sim 10^{13}$  1/s, which implies a simple decomposition mechanism.

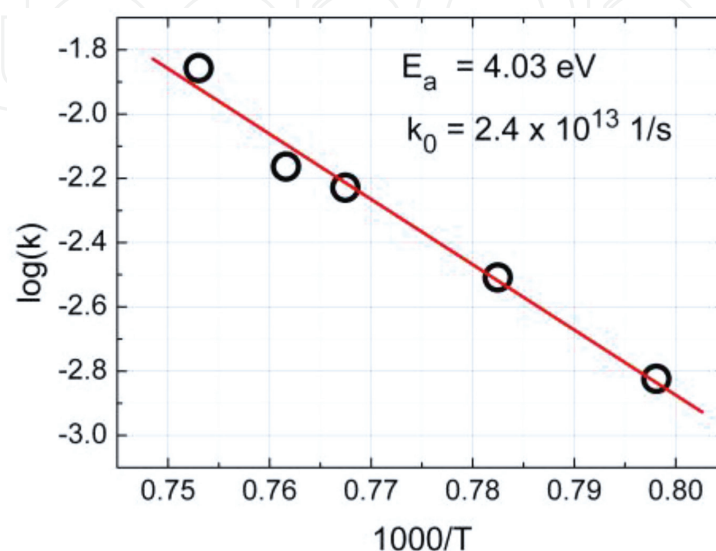


**Figure 3.**  
Arrhenius dependence of the rate constant of the ( $8 \times 8$ ) decomposition.

When the Si-N bonds break, the formation of activated  $N^*$  nitrogen atoms weakly bound to the surface and following formation of  $N_2$  ( $N^* + N^* = N_2$ ) molecules occurs. Thus, the structure ( $8 \times 8$ ) at a temperature above  $980^\circ\text{C}$  is destroyed, both during exposure to vacuum and during the continuation of nitridation process under ammonia flux, when it is converted to amorphous  $\text{Si}_3\text{N}_4$ . Indeed, at lower temperatures, the structure ( $8 \times 8$ ) is stable. Therefore, the experimental data on the transformation into an amorphous phase and thermal decomposition evidence the metastability of the phase ( $8 \times 8$ ), in contrast to the stable crystalline phase of  $\beta\text{-Si}_3\text{N}_4$  or the amorphous phase of  $\text{Si}_3\text{N}_4$ .

### 3. Comparative STM/STS study of the ( $7 \times 7$ ) and ( $8 \times 8$ ) structures on the Si (111)

#### 3.1 STM of the Si (111)-( $7 \times 7$ ) and impact of $\text{NH}_3$ adsorption

The atomic structure of the pristine surface ( $7 \times 7$ ) and the surface with chemisorbed ammonia on Si (111) (obtained at  $750^\circ\text{C}$ , 4 min,  $P_{\text{NH}_3} = 10^{-7}$  Torr) were investigated in real space by the scanning tunneling microscopy (STM) method. STM images of these surfaces are presented in **Figure 4a** and **b** (at operating parameters  $V = +1$  V and  $I = 0.025$  nA). The images were obtained in empty electronic states of silicon. Comparing images a and b in **Figure 4**, we can conclude that ammonia is adsorbed mainly to the central adatoms and rest atoms of the structure ( $7 \times 7$ ). In **Figure 4b**, it is also clearly seen that the chemisorption of ammonia induces a disorder on the surface. We consider chemisorption of ammonia as the initial process of nitridation at the silicon surface, followed by the formation of an amorphous nitride phase, since the interaction of ammonia with the dangling bonds of surface silicon atoms (111) does not change the  $sp^3$  hybridization of the orbitals of these atoms. We recall that in the amorphous phase of  $\text{Si}_3\text{N}_4$ , silicon atoms also have  $sp^3$  hybridization of orbitals.

#### 3.2 STS of the Si (111)-( $7 \times 7$ ) and impact of $\text{NH}_3$ adsorption

We performed measurements of the scanning tunneling spectroscopy (STS) of a clean surface ( $7 \times 7$ ) and on a surface with chemisorbed ammonia (**Figure 4c**). The spectra of pristine silicon surface for various characteristic points, such as corner adatoms, central adatoms, rest atoms, and hole atoms, on the Si (111)-( $7 \times 7$ ) surface are shown. Each curve for a particular characteristic point is obtained by summing 30–40 volt-ampere curves at equivalent characteristic points on the STM image. One can see a good coincidence of the STS spectra for all these characteristic points on a clean silicon surface. Peaks in the density of states for bias voltages of  $-0.3$ ,  $-0.8$ ,  $-1.5$ , and  $-2.3$  V, as well as peaks for empty states  $+0.3$  V and  $+0.8$  V, are observed. Similar peaks were observed by many groups [21, 24, 32–37], and they are usually denoted as  $S_1 = -0.3$  eV,  $S_2 = -0.8$  eV, and  $S_3 = -1.4$  eV; we also observed a state at  $-2.3$  eV, which was detected by the XPS method [38]. Some authors associate certain peaks in the density of state spectrum with specific atoms on the surface ( $7 \times 7$ ), for example, peaks at  $-0.3$  and  $+0.3$  V are associated with adatoms [21, 32], and the peak at  $-0.8$  V is associated with rest atoms [32, 37], that is, they are considered in the framework of the approximation of the local density of electronic states of a given atom. However, our experimental data, namely the presence of identical peaks for the entire family of spectra, for both adatoms and rest atoms and other characteristic points, show that these peaks on the surface of pure silicon should be considered as a manifestation of the surface two-dimensional bands of

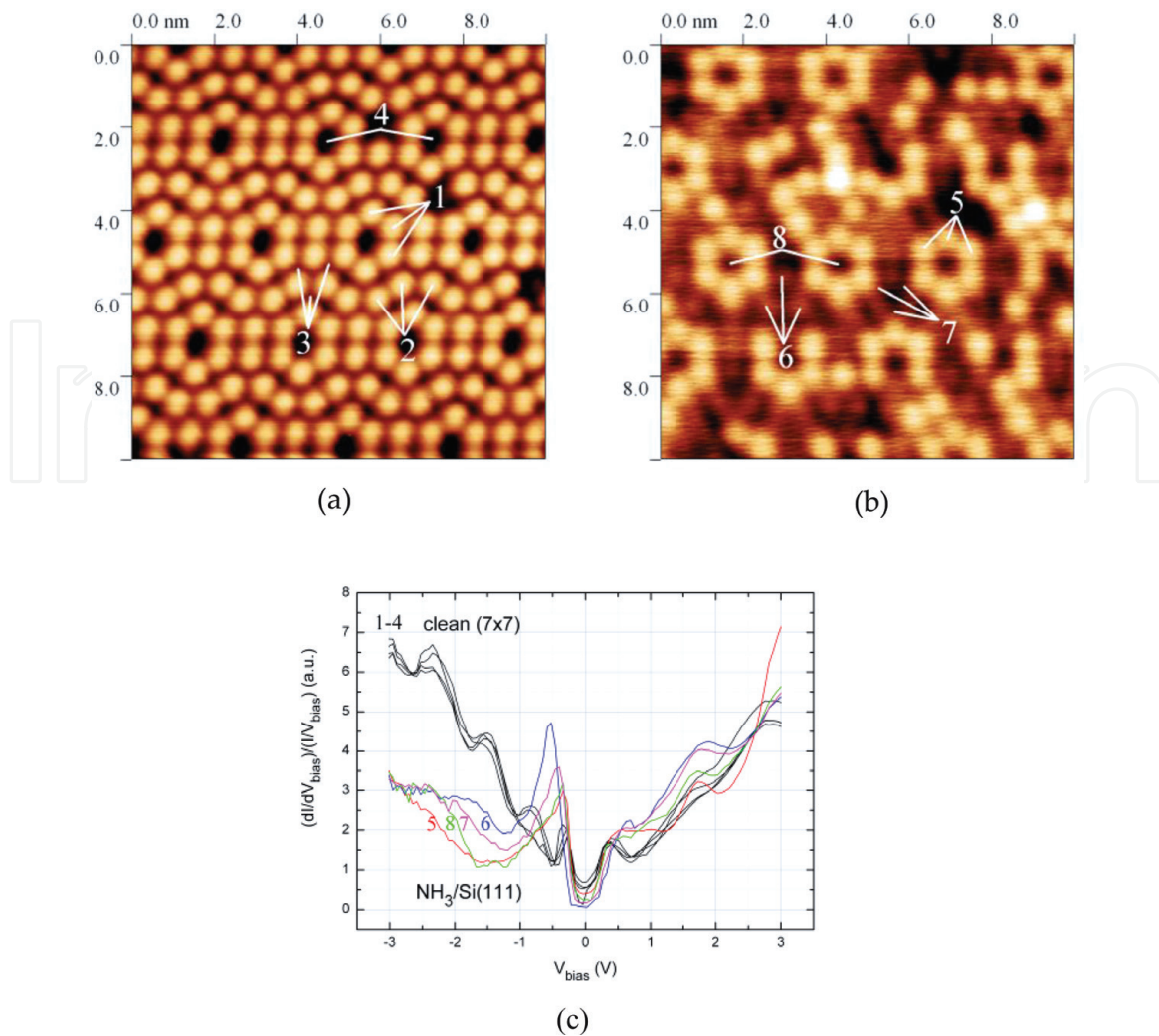


**Figure 4.**

STM images: (a) the clean surface of Si (111) with reconstruction ( $7 \times 7$ ); (b) the surface of silicon (111) treated with ammonia. The lines indicate the nearest equivalent points. (c) STS spectra of a clean surface of Si ( $7 \times 7$ ) (family of curves 1–4) and spectra after adsorption of ammonia (family of curves 5–8). Curves 1, 5, correspond to corner adatoms; 2, 6, to central adatoms; 3, 7, rest atoms; 4, 8, “corner holes”.

states of the structure ( $7 \times 7$ ). Measurements of the STS on the surface with chemisorbed ammonia show different spectra for the same family of the characteristic points. The more pronounced difference in the spectra is observed for corner and central Si adatoms, which was also manifested in STM images, as indicated above. In this case, a stronger local chemical interaction of ammonia with the central adatoms than with the corner adatoms occurs. The surface band structure of the clean surface ( $7 \times 7$ ) is destroyed. Essentially, when random Si-N chemical bonds are formed, various localized electronic states appear.

### 3.3 STM/STS of the structure ( $8 \times 8$ )

Interaction of ammonia with the (111) silicon surface at elevated temperatures (800–1150°C) results to ( $8 \times 8$ ) structure, as discussed above, in contrast to disordered structure appeared during adsorption of ammonia at lower temperatures. A typical STM image of the structure ( $8 \times 8$ ) at the working offset  $V_s = -3$  V is shown in **Figure 5a**, that is, the image in the filled states of the sample. The periodic structure ( $8/3 \times 8/3$ ) with a distance between the nearest neighboring protrusions  $a = 10.2$  Å clearly manifests itself in the figure, in agreement with numerous experimental data, see, for example [22, 23, 39]. In addition, in **Figure 5a**, a honeycomb structure is clearly observed, with a hexagon whose side  $b$  is approximately 6 Å in



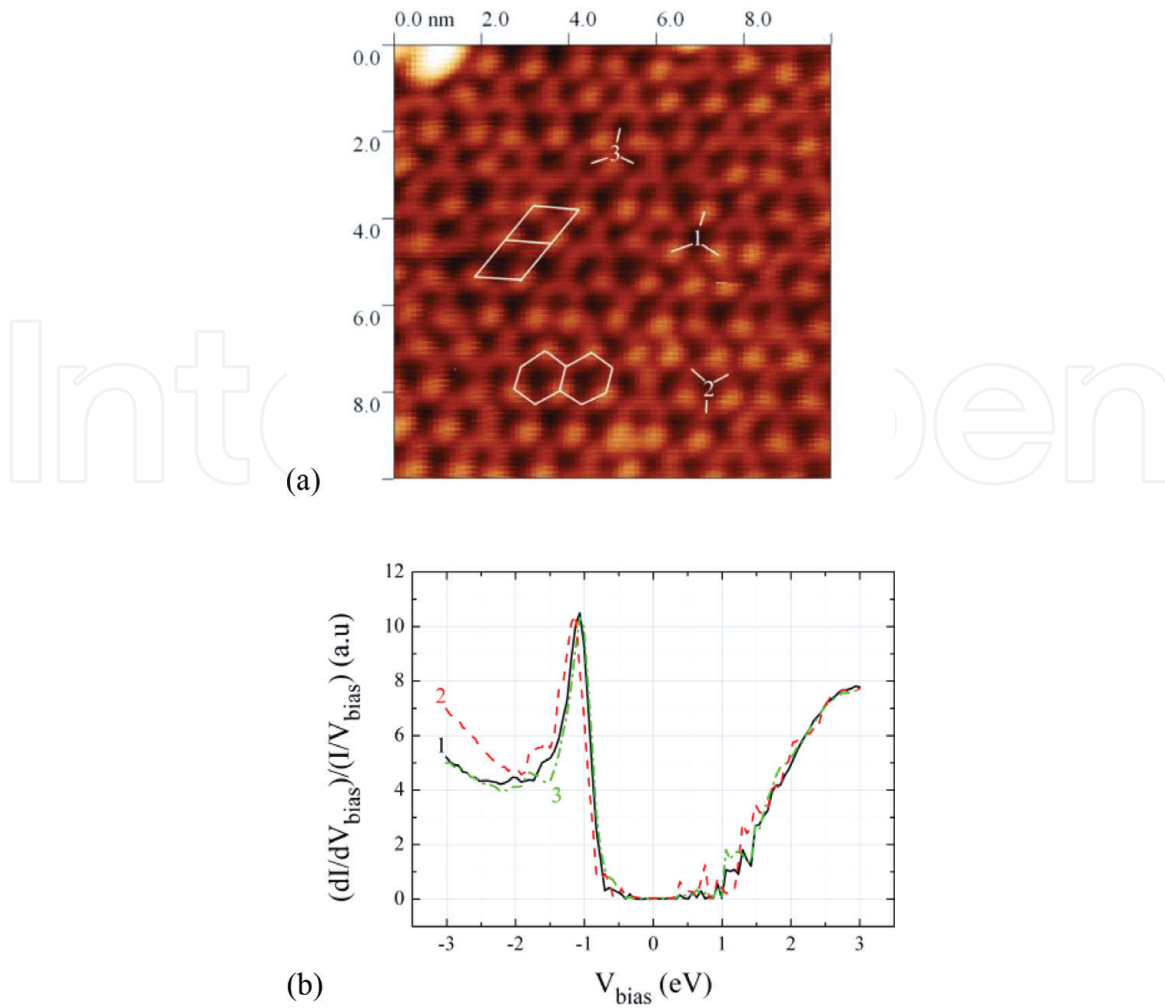


**Figure 5.**

(a) STM image of the structure ( $8 \times 8$ ). The white figures are marking elementary cells ( $8/3 \times 8/3$ ) and hexagons; (b) STS spectra measured for three characteristic points: 1. protrusion, 2. the vertices of hexagon that not occupied by protrusion, 3. center of hexagon (corresponding three characteristic points are marked in Figure 5a).

length and rotated at  $30^\circ$  relative to the unit cell of ( $8/3 \times 8/3$ ). **Figure 5b** clearly shows that the protrusions of the phase ( $8/3 \times 8/3$ ) are brighter than the “vertices” and “sides” of the hexagons. Consequently, the protrusions ( $8/3 \times 8/3$ ) lie on top of the honeycomb structure. In our opinion, protrusions correspond to an ordered adsorption phase, which occupy only three of the six vertices of the hexagons. The relationship between the side length of a hexagon and the distance between protrusions is defined by the expression  $a = 2 \times b \times \cos(30^\circ)$ . It is clear that the periodicities of adsorption phase and hexagons are the same. There are vacancies in the adsorption phase. This confirms the high mobility of atoms in the adsorption phase, which was noted in the work [24]. At present, it is difficult to unequivocally indicate the nature of the protrusions, perhaps they consist of one, two, or several silicon atoms [40, 41]. For the current study, the hexagonal structure is most interesting, since it determines an atomic arrangement in the structure ( $8 \times 8$ ).

The authors of the work [24] also have observed a honeycomb structure and have explained it by the manifestation of the crystal structure of  $\beta\text{-Si}_3\text{N}_4$ . The size of the hexagon side in the STM images represented by the authors (see **Figure 5a** and **b** in the article [24]), as well as in our case, was about  $6 \text{ \AA}$ . Let us recall that in the crystal structure of  $\beta\text{-Si}_3\text{N}_4$ , there is a characteristic fragment—a “small” hexagon with a side of  $2.75 \text{ \AA}$ , as shown experimentally, for example, in work [42] with the help of high-resolution TEM. The hexagonal periodic structure with lattice constant of  $7.62 \text{ \AA}$  of the  $\beta\text{-Si}_3\text{N}_4$  is constructed of these “small” hexagons, but there are no hexagons with

the 6 Å side in the structure. Consequently, the honeycomb structure detected in this work and in the work [24] does not correspond to the structure of the  $\beta$ - $\text{Si}_3\text{N}_4$  crystal. It seems that in most studies devoted to STM of the  $(8 \times 8)$  structure, only the adsorption phase  $(8/3 \times 8/3)$  was clearly observed because usually the ordering of the structure is not very high due to the mobility of adatoms (see [21, 24]); hence, the 6 Å honeycomb structure did not be taken into account until now at the modeling of  $(8 \times 8)$  structure.

**Figure 5b** shows the STS spectra measured for three different characteristic points: 1. the protrusions, 2. the vertices of the hexagons that not occupied by the protrusions, and 3. the centers of the hexagons. Each curve is obtained by averaging of 30–40 equivalent points. There is a good coincidence of the curves for various characteristic points, as might be expected for a periodic structure. In our opinion, the position of the peak in the density of states at  $-1.1$  eV corresponds to the maximum of the valence band for the surface periodic structure  $(8 \times 8)$ . The band gap of the structure  $(8 \times 8)$  is about 2.2 eV, and it is determined by the energy gap between the bonding  $\pi$  and antibonding  $\pi^*$  orbitals (as discussed below). The band gap of 2.2 eV is much less than the band gap of crystalline  $\beta$ - $\text{Si}_3\text{N}_4$  or amorphous  $\text{Si}_3\text{N}_4$  (4.9–5.3 eV). For comparison, **Figure 6** shows the spectra of a pristine silicon surface with  $(7 \times 7)$  reconstruction (curve 1), the structure  $(8 \times 8)$  (curve 2), and a thin amorphous  $\text{Si}_3\text{N}_4$  layer (curve 3). The STS spectrum of the amorphous phase of  $\text{Si}_3\text{N}_4$  has a characteristic peak at energy of about  $-4$  eV, which is observed by many groups [21, 24, 43–45]. The authors of [21, 43] refer it to adsorbed nitrogen atoms on the surface, but since this peak exists in thick crystalline  $\beta$ - $\text{Si}_3\text{N}_4$  and amorphous  $\text{Si}_3\text{N}_4$  layers, as demonstrated in works [24, 44, 45], this peak corresponds to the valence-band maximum of bulk  $\text{Si}_3\text{N}_4$ ; by the other words, it is the highest occupied molecular orbital (HOMO) of  $\sigma$  bonding band.

The peak at  $-1.1$  eV of the structure  $(8 \times 8)$  (curve 2) corresponds to the  $\pi$  orbitals, since it has the highest energy among the occupied electron states HOMO and this peak is much higher than peak of  $\sigma$  bonding band ( $-4$  eV) [46]; moreover, this peak is absent in the spectrum of amorphous  $\text{Si}_3\text{N}_4$ . The peak at  $-1.1$  eV was also observed by the method of photoelectron spectroscopy (PES) in [47]. However, the authors attributed it to the dangling silicon or nitrogen bonds of  $\beta$ - $\text{Si}_3\text{N}_4$  phase within the framework of the generally accepted concept of the  $(8 \times 8)$  structure description as a  $\beta$ - $\text{Si}_3\text{N}_4$  crystal. However, in **Figure 5** of the work [47],

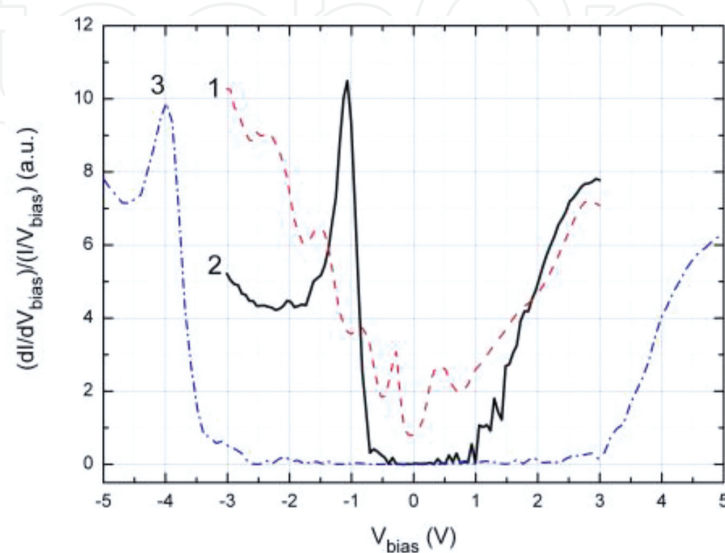


**Figure 6.** Scanning tunneling spectra: 1. of the clean silicon surface of Si (111) with reconstruction  $(7 \times 7)$ ; 2. of the structure  $(8 \times 8)$ ; and 3. of the amorphous phase  $\text{Si}_3\text{N}_4$ .

an appreciable difference in the electronic structures (state densities)  $\beta$ - $\text{Si}_3\text{N}_4$  and  $(8 \times 8)$  is seen. Moreover, in the works [48, 49], devoted to the calculation of electronic states (0001)  $\beta$ - $\text{Si}_3\text{N}_4$ , HOMO states associated with dangling bonds did not found. As it will be shown further, it is better to associate this peak in the density of states  $(8 \times 8)$  with  $\pi$ -band.

#### 4. HRTEM study of van der Waals structure of silicon nitride and aluminum nitride

The atomic arrangement of  $(8 \times 8)$  was also investigated here by the HRTEM method. For these studies, samples with the following sequence of layers were grown on the (111) Si substrate: 2–3 monolayers of silicon nitride with a structure  $(8 \times 8)$  and thin epitaxial layer of AlN. The interplanar spacing in the Si substrate in the silicon nitride and AlN layers was determined, see **Figure 7**. It turned out that the interplanar spacing between the layers of silicon nitride and also between the last silicon layer and the silicon nitride layer is about  $3.3 \text{ \AA}$ , which is noticeably larger than the interplanar distances in silicon ( $3.13 \text{ \AA}$ ) and the known thickness of the  $\beta$ - $\text{Si}_3\text{N}_4$  monolayer ( $2.9 \text{ \AA}$ ). In addition, the layers of silicon nitride differ sharply in contrast from the layers of Si and AlN.

The interplanar distances in silicon nitride of  $3.3 \text{ \AA}$  are larger than the interplanar distances Si  $3.13 \text{ \AA}$  and are larger than the thickness of the monolayer  $\beta$ - $\text{Si}_3\text{N}_4$  ( $2.9 \text{ \AA}$ ). The interplanar distances in the epitaxial AlN layer are also larger than normal interplanar distances in bulk wurtzite AlN ( $2.49 \text{ \AA}$ ). Therefore, this epitaxial structure  $(\text{SiN})_2(\text{AlN})_4$  turned out to be a van der Waals crystal.

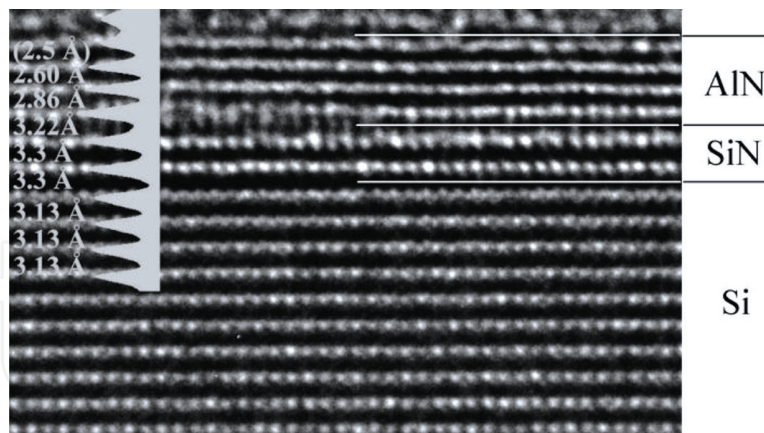


**Figure 7.**  
HRTEM image of layers of SiN and AlN on the Si (111) surface.

#### 5. Graphene-like models of the structure $(8 \times 8)$

The increase in the interplanar distance in silicon nitride, detected by the HRTEM method, is a consequence of the weaker (van der Waals) interaction between the atomic planes. The interaction between the silicon nitride layer and the Si substrate also turned out to be weaker than interaction provided by normal covalent bonds. As mentioned above, when the structure  $(8 \times 8)$  is formed, the ammonia interaction occurs with the mobile silicon adatoms, but not with the dangling bonds of the silicon atoms on the surface, which provides an increased

interlayer distance between the silicon nitride layer and the silicon surface. Taking into account all the experimental data presented, it can be assumed that the structure ( $8 \times 8$ ) has a graphene-like nature. Moreover, the production of graphene-like AlN layers, described in our paper [50], was possible only on such a graphene-like layer of silicon nitride. If only the silicon nitride layer had dangling bonds (silicon or nitrogen), then the AlN layer would have formed in the bulk wurtzite structure (formation of graphene-like AlN is discussed below). Possible graphene-like models of the layer of silicon nitride  $g\text{-Si}_3\text{N}_4$  and  $g\text{-Si}_3\text{N}_3$  are shown in **Figure 8**. Similar model  $g\text{-Si}_3\text{N}_3$  was considered earlier in the theoretical work of Guo [51]. The basis of both structures is the  $\text{Si}_3\text{N}_3$  aromatic conjugated rings connected to each other by either nitrogen atoms (**Figure 8a**) having  $sp^2$  hybridization (as in the  $\beta\text{-Si}_3\text{N}_4$  crystal structure) or via Si-Si bonds (**Figure 8b**). Atoms of silicon in these structures have  $sp^2$  hybridization of atomic orbitals, forming three  $\sigma$ -bonds in planar configuration. The fourth electron of the silicon participates in the  $\pi$ -bond with the nitrogen atom in the ring. Each nitrogen atom uses three valence electrons, and in the aromatic ring, nitrogen has  $sp$  hybridization, and the third valence electron participates in the  $\pi$ -bond.

The proposed structures satisfy the available experimental diffraction data, STM/STS, and HRTEM. They reproduce the periodicity ( $8 \times 8$ ) and the characteristic features of the honeycomb structure observed in the STM, taking into account the weakening of interaction with the silicon surface (there are no dangling bonds in the layer) and explaining the metastability of the structure ( $8 \times 8$ ). Metastability is a consequence of the formation of weaker  $\pi$ -bonds than  $\sigma$ -bonds. In the stable structure of  $\text{Si}_3\text{N}_4$  (amorphous or crystalline  $\beta\text{-Si}_3\text{N}_4$ ), all bonds of silicon and nitrogen are  $\sigma$ -bonds.

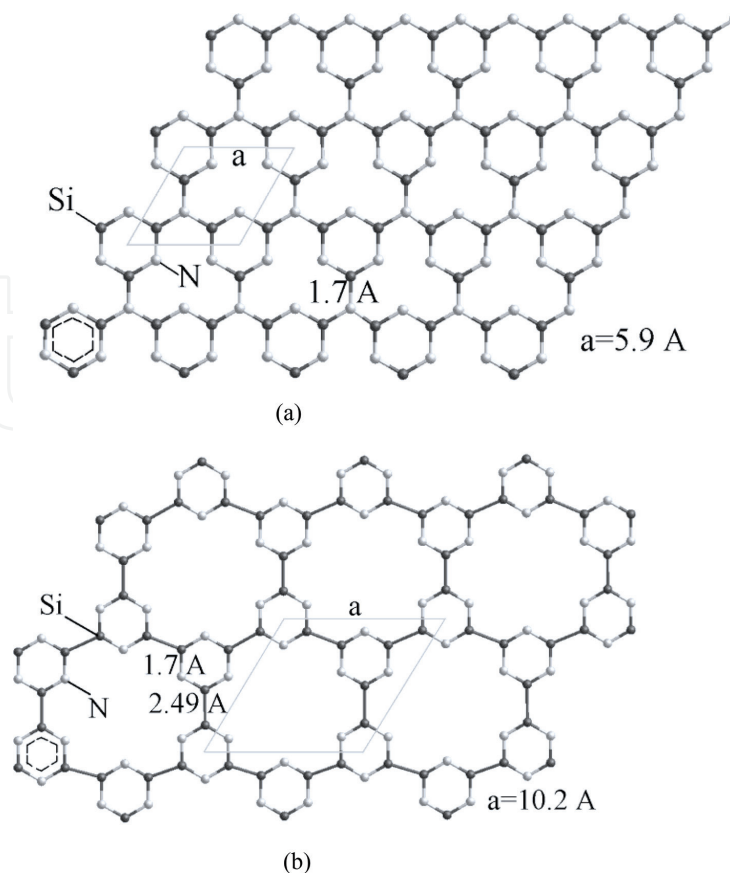


**Figure 8.** Models of a graphene-like layer of silicon nitride. (a)  $g\text{-Si}_3\text{N}_4$ ; (b)  $g\text{-Si}_3\text{N}_3$ .

## 6. Graphene-like AlN layer formation on Si (111) surface by ammonia MBE

In the present experiments, an AlN flat ultrathin layer was prepared by using the following two-stage procedure. At first, a clean ( $1 \times 1$ ) silicon surface was exposed under the ammonia flux (10 sccm) at the substrate temperatures of  $1050^\circ\text{C}$ , and in the second stage, the AlN layer is formed by the Al deposition when the ammonia flux was switched off and the background ammonia pressure of  $\sim 10^{-7}$ – $10^{-8}$  Torr was achieved.

For the AlN formation, the ammonia flux was turned off at the moment when the best ( $8 \times 8$ ) RHEED pattern with sharp and bright eightfold fractional spots was reached. This moment corresponds to the maximum of the curve in **Figure 1b**. Next, the Al deposition onto the highly ordered ( $8 \times 8$ ) structure was performed. The Al flux was established on the value equivalent to the AlN growth rate of  $\sim 0.1$  ML/s. The appearance of the AlN diffraction spots and the transformation of the ( $8 \times 8$ ) structure to a new fourfold structure was observed. The RHEED pattern of AlN and ( $4 \times 4$ ) structure is shown in **Figure 9a**. An intensity profile measured along a horizontal line (A-B) crossing the streaks is shown in **Figure 9b**.

The observed fundamental (0-1) AlN streak position exactly coincides with the position of the fractional spot (0-5/4); see **Figure 9b**). Then, an AlN in-plane lattice constant was calculated from the relationship  $4 \times a_{111\text{Si}} = 5 \times a_{\text{AlN}}$ , where  $a_{111\text{Si}} = 3.85 \text{ \AA}$ . Hence, the calculated lattice constant is  $a_{\text{AlN}} = 3.08 \text{ \AA}$ . This value

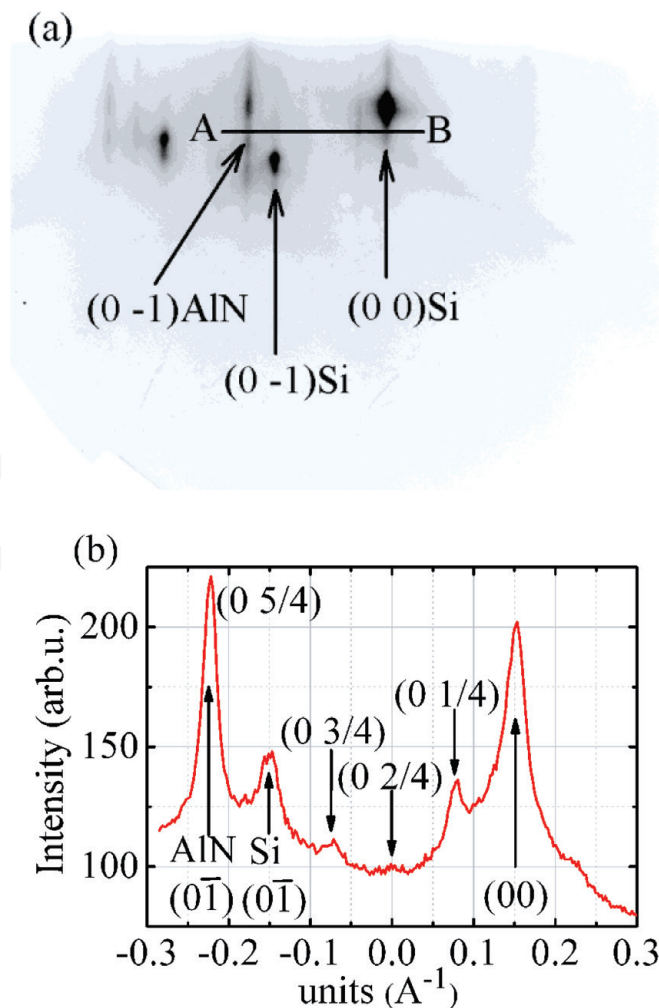


**Figure 9.** (a) RHEED pattern of the Si surface ( $4 \times 4$ ); (b) the intensity profile of ( $4 \times 4$ ) structure measured along the line (A-B) crossing the diffraction streaks, from [50].

is substantially lower than lateral lattice constant of the bulk wurtzite AlN value being 3.125 Å, which has been measured by the X-ray diffraction method at a high temperature [52].

The (4 × 4) structure is not the consequence of the actual reconstruction of the Si (111) surface. The fractional spots (0 1/4), (0 2/4), and (0 3/4) (and others) are detectable in the RHEED pattern (Figure 9) as the result of electrons scattering by both the Si and g-AlN crystal lattices, that is, mixing of reciprocal vectors of these lattices. For example, the fractional reciprocal vectors  $q(0\ 1/4)$  is a result of relation  $q(0\ 1/4) = q(0\ 1)_{\text{AlN}} - q(0\ 1)_{\text{Si}}$ , where  $q(0\ 1)_{\text{AlN}}$  and  $q(0\ 1)_{\text{Si}}$  are integer order reciprocal vectors of g-AlN and Si, respectively. The approximate equality of the fourfold silicon lateral constant and the fivefold wurtzite AlN lateral constant was previously pointed out in some studies (e.g., see paper [53, 54]) with mismatch of ~1.3%. In our case, there is an exact coincidence, and as the result, the fractional beams of (4 × 4) structure are experimentally observed in the RHEED pattern. Thus, an extremely thin and flat of AlN on (111) Si substrate with the lattice constant of  $a = 3.08\ \text{\AA}$  is prepared. This value is close to the *ab initio* calculated value of 3.09 Å for the graphene-like aluminum nitride lattice with  $sp^2$ -like bonding [55, 56].

There is only one more experimental work [57] that dedicated to epitaxial growth of graphite-like hexagonal AlN nanosheets on single crystal Ag (111). It is interesting to note that a simple our calculation of the g-AlN lattice constant using the lateral constant of (111) Ag (2.89 Å) from the diffraction pattern presented by authors of the work gives the value in the range of 3.06–3.09 Å in contrast to the value presented by the authors of 3.13 Å.

We have carried out experimental precise measurements of the in-plane AlN lattice constant under the Al and NH<sub>3</sub> fluxes supplied onto the surface either separately or simultaneously. The evolution of in-plane lattice constant during the g-AlN formation process is depicted in Figure 10. The increasing of the lattice constant from 3.08 to 3.09 Å under Al flux without ammonia flux (i.e., there is no growth of AlN) is clearly visible.

Then, the Al flux was turned off (at the moment of 340 s) and the NH<sub>3</sub> flux (10 sccm) was switched on. The lateral lattice constant of g-AlN was keeping the same value of 3.09 Å, and so, under the ammonia flux, the formed g-AlN is quite stable. The lateral size of the g-AlN islands has been estimated from the RHEED data as ~70–100 Å.

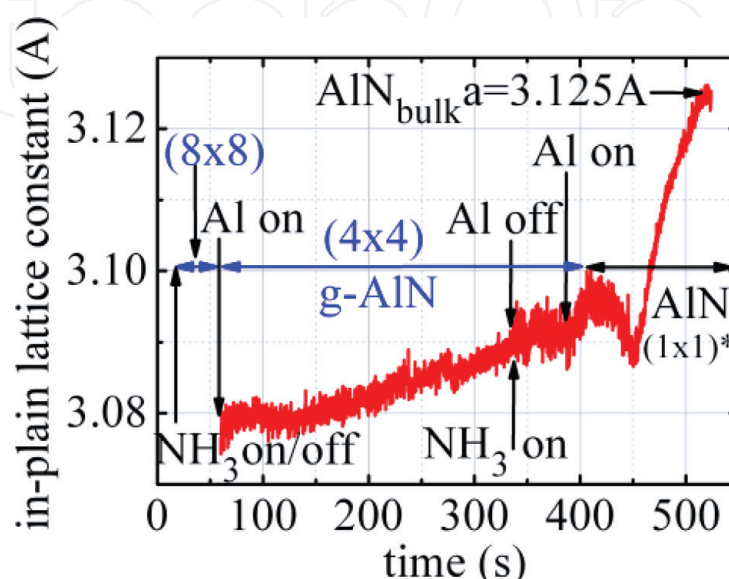
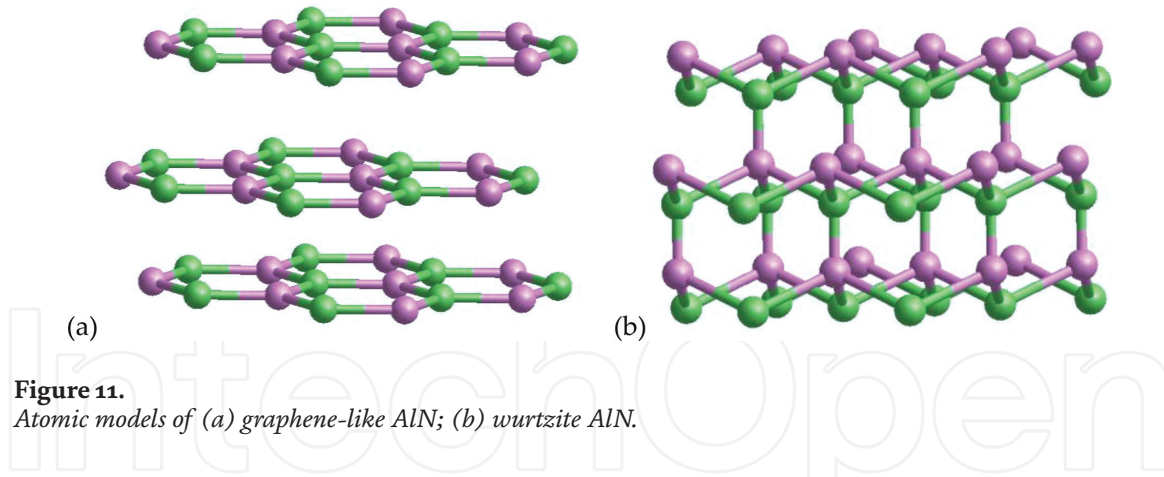


Figure 10.  
Evolution of an in-plane lattice constant during the g-AlN formation process.



**Figure 11.** Atomic models of (a) graphene-like AlN; (b) wurtzite AlN.

The epitaxial growth of AlN was initiated by turning on the Al flux, keeping the same ammonia flux (at the moment of 390 s). The fractional streaks of the  $(4 \times 4)$  structure are gradually dimmed together with the increasing of the fundamental  $(0\ 1)$  g-AlN streak intensity. At the moment of about 420 s, a structure  $(1 \times 1)$  of g-AlN appears. Further growth of AlN leads to the lattice constant conversion from 3.09 to 3.125 Å. The value 3.125 Å corresponds to bulk value of the wurtzite AlN lattice constant at high temperature [52].

Thus, the transformation from graphite-like ( $sp^2$ -hybridization, see **Figure 11a**) to wurtzite structure of AlN ( $sp^3$ -hybridization, **Figure 11b**) is observed. This transition is similar to the transition metastable graphene-like silicon nitride of the structure  $(8 \times 8)$  to stable amorphous phase a- $Si_3N_4$ . The maximal thickness of the g-AlN layer of  $\sim 5$ – $6$  AlN monolayers was estimated using the AlN growth rate that is less than the theoretically predicted value of 22–24 monolayer [58]. The difference between calculations and experimental data might be attributed to the competition with the bulk stabilization mechanism involving structural defects and roughening, which were not taken into account in work [58]. The similar discrepancy between theoretically predicted and experimentally measured thickness of the  $sp^2$ - $sp^3$  transition was noticed for ZnO [59].

## 7. Conclusion

Systematic studies of the structure  $(8 \times 8)$  by the methods RHEED, STM/STS, and HRTEM were carried out. It is found that the structure  $(8 \times 8)$  is formed within 5–7 s during nitridation of the Si (111) surface at the temperature range 950–1150°C. The formation rate of the structure  $(8 \times 8)$  is independent on the temperature. The kinetics of the thermal decomposition of this two-dimensional layer of silicon nitride has been studied. It is established that the structure  $(8 \times 8)$  is a metastable phase, and with further nitridation, a transition to the stable amorphous phase of  $Si_3N_4$  occurs. In the structure  $(8 \times 8)$ , the honeycomb structure with the side length of hexagon of 6 Å was found for the first time, on which the adsorption phase of silicon is located with a periodicity of 10.2 Å. The interplanar spacing in the epitaxial structure  $(SiN)_2(AlN)_4$  on the (111) Si surface are measured: 3.3 Å in silicon nitride layer and 2.86 Å in AlN. These interlayer distances correspond to the weak van der Waals interaction between the layers. Scanning tunneling spectroscopy in the filled states revealed a peak of 1.1 eV below the Fermi level. Comparison of the measurements in the STS of the metastable phase of silicon nitride with measurements made on a clean surface of Si (111)– $(7 \times 7)$  and on an amorphous  $Si_3N_4$  layer helped us in identifying the peak  $-1.1$  eV as the  $\pi$ -bonding band of the structure  $(8 \times 8)$ . The band gap between the bonding and antibonding orbitals is

	Lateral lattice constant	Interplanar spacing	Heat of formation	Band gap
g-Si <sub>3</sub> N <sub>3</sub> (g-Si <sub>3</sub> N <sub>4</sub> )	10.2 Å (5.9 Å hex side)	3.3 Å	< 4 eV	2.2 eV
g-AlN	3.08 Å	2.86 Å		~ 3.0 eV [55]

**Table 1.**  
*Structural and thermodynamic characteristics of g-AlN and g-Si<sub>3</sub>N<sub>3</sub>.*

found of 2.2 eV. Consequently, the 2D silicon nitride layer is a semiconductor. The data obtained allowed us to propose new graphene-like model structures (8 × 8). The models are planar graphene-like structures of g-Si<sub>3</sub>N<sub>3</sub> and/or g-Si<sub>3</sub>N<sub>4</sub>. Owing to the formation of graphene-like Si<sub>3</sub>N<sub>3</sub> layer, it is possible to synthesize graphene-like g-AlN, the lateral lattice constant of 3.08 Å, and the interplanar distance of 2.86 Å. When the AlN thickness of 5–6 monolayers is reached, g-AlN passes into the wurtzite structure.

**Table 1** summarizes some important characteristics of graphene-like phases of silicon nitride and aluminum nitride.

## Acknowledgements

This work was supported by the Russian Foundation for Basic Research (Grant Nos. 17-02-00947, 18-52-00008).

## Author details


Vladimir G. Mansurov<sup>1\*</sup>, Yuriy G. Galitsyn<sup>1</sup>, Timur V. Malin<sup>1</sup>, Sergey A. Teys<sup>1</sup>, Konstantin S. Zhuravlev<sup>1</sup>, Ildiko Cora<sup>2</sup> and Bela Pecz<sup>2</sup>

<sup>1</sup> Rzhanov Institute of Semiconductor Physics Siberian Branch of Russian Academy of Sciences, Novosibirsk, Russia

<sup>2</sup> Thin Film Physics Department, Institute of Technical Physics and Materials Science Centre for Energy Research, Hungarian Academy of Sciences, Budapest, Hungary

\*Address all correspondence to: mansurov@isp.nsc.ru

## IntechOpen

© 2018 The Author(s). Licensee IntechOpen. This chapter is distributed under the terms of the Creative Commons Attribution License (<http://creativecommons.org/licenses/by/3.0>), which permits unrestricted use, distribution, and reproduction in any medium, provided the original work is properly cited. 



## References

- [1] Du A, Sanvito S, Smith SC. First-principles prediction of metal-free magnetism and intrinsic half-metallicity in graphitic carbon nitride. *Physical Review Letters*. 2012;**108**:197207
- [2] Huynh MH, Hiskey MA, Archuleta JG, Roemer EL. Preparation of nitrogen-rich nanolayered, nanoclustered, and nanodendritic carbon nitrides. *Angewandte Chemie*. 2005;**117**:747-749
- [3] Li X, Zhang S, Wang Q. Stability and physical properties of a tri-ring based porous g-C<sub>4</sub>N<sub>3</sub> sheet. *Physical Chemistry Chemical Physics*. 2013;**15**:7142-7146
- [4] Niu P, Liu G, Cheng HM. Nitrogen vacancy-promoted photocatalytic activity of graphitic carbon nitride. *Journal of Physical Chemistry C*. 2012;**116**:11013-11018
- [5] Niu P, Zhang L, Liu G, Cheng HM. Graphene-like carbon nitride nanosheets for improved photocatalytic activities. *Advanced Functional Materials*. 2012;**22**:4763-4770
- [6] Wang X, Blechert S, Antonietti M. Polymeric graphitic carbon nitride for heterogeneous photocatalysis. *ACS Catalysis*. 2012;**2**:1596-1606
- [7] Li X, Zhou J, Wang Q, Kawazoe Y, Jena P. Patterning graphitic C–N sheets into a kagome lattice for magnetic materials. *Journal of Physical Chemistry Letters*. 2013;**4**:259-263
- [8] Teter DM, Hemley RJ. Low-compressibility carbon nitrides. *Science*. 1996;**271**:53-55
- [9] Botari T, Huhn WP, Lau VW, Lotsch BV, Blum V. Thermodynamic equilibria in carbon nitride photocatalyst materials and conditions for the existence of graphitic carbon nitride g-C<sub>3</sub>N<sub>4</sub>. *Chemistry of Materials*. 2017;**29**:4445-4453
- [10] Algara-Siller G, Severin N, Chong SY, Björkman T, Palgrave RG, Laybourn A, et al. Triazine-based graphitic carbon nitride: A two-dimensional semiconductor. *Angewandte Chemie*. 2014;**53**:7450-7455
- [11] Kim KK, Hsu A, Jia X, Kim SM, Shi Y, Hofmann M, et al. Synthesis of monolayer hexagonal boron nitride on Cu foil using chemical vapor deposition. *Nano Letters*. 2012;**12**:161-166
- [12] Ismach A, Chou H, Ferrer DA, Wu Y, McDonnell S, Floresca HC, et al. Toward the controlled synthesis of hexagonal boron nitride films. *ACS Nano*. 2012;**6**(7):6378-6385
- [13] Houssa M, Pourtois G, Afanas'ev VV, Stesmans A. Can silicon behave like graphene? A first-principles study. *Applied Physics Letters*. 2010;**97**:112106
- [14] Moslehi MM, Saraswat KC. Thermal nitridation of Si and SiO<sub>2</sub> for VLSI. *IEEE Journal of Solid-State Circuits*. 1985;**20**:26-43
- [15] Murarka SP, Chang CC, Adams AC. Thermal nitridation of silicon in ammonia gas: Composition and oxidation resistance of the resulting films. *Journal of the Electrochemical Society*. 1979;**126**:996-1003
- [16] Hayafuji Y, Kajiwara K. Nitridation of silicon and oxidized-silicon. *Journal of the Electrochemical Society*. 1982;**129**:2102-2108
- [17] Wu CY, King CW, Lee MK, Tchen CT. Growth kinetics of silicon thermal nitridation. *Journal of the Electrochemical Society*. 1982;**129**:1559-1563
- [18] Schrott AG, Fain SC. Nitridation of Si(111) by nitrogen atoms II. *Surface Science*. 1982;**123**:204-222

- [19] van Bommel AJ, Meyer F. A low energy electron diffraction study of the PH<sub>3</sub> adsorption on the Si (111) surface. *Surface Science*. 1967;**8**:381-398
- [20] Rottger B, Kliese R, Neddermeyer H. Adsorption and reaction of NO on Si(111) studied by scanning tunneling microscopy. *Journal of Vacuum Science and Technology B*. 1996;**14**:1051-1054
- [21] Ahn H, Wu CL, Gwo S, Wei CM, Chou YC. Structure determination of the Si<sub>3</sub>N<sub>4</sub>/Si(111)-(8×8) Surface: A combined study of kikuchi electron holography, scanning tunneling microscopy, and *ab initio* calculations. *Physical Review Letters*. 2001;**86**:2818-2821
- [22] Wang XS, Zhai G, Yang J, Cue N. Crystalline Si<sub>3</sub>N<sub>4</sub> thin films on Si(111) and the 4×4 reconstruction on Si<sub>3</sub>N<sub>4</sub>(0001). *Physical Review B*. 1999;**60**:R2146-R2149
- [23] Wang XS, Zhai G, Yang J, Wang L, Hu Y, Li Z, et al. Nitridation of Si(111). *Surface Science*. 2001;**494**:83-94
- [24] Flammini R, Allegrini P, Wiame F, Belkhou R, Ronci F, Colonna S, et al. Nearly-free electron like surface resonance of a β-Si<sub>3</sub>N<sub>4</sub>(0001)/Si(111)-8×8 interface. *Physical Review B*. 2015;**91**:075303
- [25] Mansurov VG, Malin TV, Galitsyn YG, Shklyaev AA, Zhuravlev KS. Kinetics and thermodynamics of Si(111) surface nitridation in ammonia. *Journal of Crystal Growth*. 2016;**441**:12-17
- [26] Jennings HM, Edwards JO, Richman MH. Molecular structure, microstructure, macrostructure and properties of silicon nitride. *Inorganica Chimica Acta*. 1976;**20**:167-181
- [27] Rogilo DI, Fedina LI, Kosolobov SS, Ranguelov BS, Latyshev AV. Critical terrace width for two-dimensional nucleation during Si growth on Si(111)-(7×7) surface. *Physical Review Letters*. 2013;**111**:036105
- [28] Sitnikov S, Kosolobov S, Latyshev A. Attachment–detachment limited kinetics on ultra-flat Si(111) surface under etching with molecular oxygen at elevated temperatures. *Surface Science*. 2015;**633**:L1-L5
- [29] Sitnikov SV, Latyshev AV, Kosolobov SS. Advacancy-mediated atomic steps kinetics and two-dimensional negative island nucleation on ultra-flat Si(111) surface. *Journal of Crystal Growth*. 2017;**457**:196-201
- [30] Shetty S, Kesaria M, Ghatak J, Shivaprasad SM. The origin of shape, orientation, and structure of Spontaneously formed Wurtzite GaN nanorods on cubic Si(001) Surface. *Crystal Growth and Design*. 2013;**13**:2407-2412
- [31] Batha HD, Whitney ED. Kinetics and mechanism of the thermal decomposition of Si<sub>3</sub>N<sub>4</sub>. *Journal of the American Ceramic Society*. 1973;**56**:365-369
- [32] Wolkow R, Avouris P. Atom-resolved surface chemistry using scanning tunneling microscopy. *Physical Review Letters*. 1988;**60**:1049-1052
- [33] Brommer KD, Galvan M, Dal Pino A, Joannopoulos JD. Theory of adsorption of atoms and molecules on Si(111)-(7×7). *Surface Science*. 1994;**314**:57-70
- [34] Lim H, Cho K, Park I, Joannopoulos JD, Kaxiras E. *Ab initio* study of hydrogen adsorption on the Si(111)-(7×7) surface. *Physical Review B*. 1995;**52**:17231-17237
- [35] Chen L, Pan BC, Xiang H, Wang B, Yang J, Hou JG, et al. Observation of local electronic structures of adatom

- vacancies in Si(111)–(7×7) surface in real space. *Physical Review B*. 2007;**75**:085329
- [36] Odobescu AB, Maizlakh AA, Zaitsev-Zotov SV. Electron correlation effects in transport and tunneling spectroscopy of the Si(111)–7×7 surface. *Physical Review B*. 2015;**92**:165313
- [37] Siriwardena HD, Yamashita T, Shimomura M. STM Observation of the Si(111)-(7×7) reconstructed surface modified by excess phosphorus doping. *International Journal of Electrical and Computer Engineering*. 2017;**7**:2993-3001
- [38] Losio R, Altmann KN, Himpsel FJ. Continuous transition from two- to one-dimensional states in Si(111)-(5×2)–Au. *Physical Review Letters*. 2000;**85**:808-811
- [39] Morita Y, Tokumoto H. Origin of the 8/3×8/3 superstructure in STM images of the Si(111)-8×8: N surface. *Surface Science Letters*. 1999;**443**:L1037-L1042
- [40] Binggeli N, Chelikowsky JR. Langevin molecular dynamics with quantum forces: Application to silicon clusters. *Physical Review B*. 1994;**50**:11764-11770
- [41] Dixon DA, Feller D, Peterson KA, Gole JL. The molecular structure and ionization potential of Si<sub>2</sub>: The role of the excited states in the photoionization of Si<sub>2</sub>. *Journal of Physical Chemistry A*. 2000;**104**:2326-2332
- [42] Ziegler A, Kisielowski C, Ritchie RO. Imaging of the crystal structure of silicon nitride at 0.8 Angstrom resolution. *Acta Materialia*. 2002;**50**:565-574
- [43] Wu C, Chen W, Su Y. N<sub>2</sub>-plasma nitridation on Si(111): Its effect on crystalline silicon nitride growth. *Surface Science*. 2012;**606**:L51-L54
- [44] Xu Y, Ching WY. Electronic structure and optical properties of α and β phases of silicon nitride, silicon oxynitride, and with comparison to silicon dioxide. *Physical Review B*. 1995;**51**:17379-17389
- [45] Gritsenko VA. Electronic structure of silicon nitride. *Physics-Uspekhi*. 2012;**55**:498-507
- [46] Giuliani M, Motta N. Polymer self-assembly on carbon nanotubes. In: Belucci S, editor. *Self-Assembly of Nanostructures The INFN lectures Vol. III*. New York: Springer; 2012
- [47] Kim JW, Yeom HW. Surface and interface structures of epitaxial silicon nitride on Si(111). *Physical Review B*. 2003;**67**:035304
- [48] Bagatur'yants AA, Novoselov KP, Safonov AA, Cole JV, Stoker M, Korkin AA. Silicon nitride chemical vapor deposition from dichlorosilane and ammonia: Theoretical study of surface structures and reaction mechanism. *Surface Science*. 2001;**486**:213-225
- [49] Bermudez VM. Theoretical study of the electronic structure of the Si<sub>3</sub>N<sub>4</sub>(0001) surface. *Surface Science*. 2005;**579**:11-20
- [50] Mansurov V, Malin T, Galitsyn Y, Zhuravlev K. Graphene-like AlN layer formation on (111)Si surface by ammonia molecular beam epitaxy. *Journal of Crystal Growth*. 2015;**428**:93-97
- [51] Guo Y, Zhang S, Wang Q. Electronic and optical properties of silicon based porous sheets. *Physical Chemistry Chemical Physics*. 2014;**16**:16832-16836. DOI: 10.1039/C4CP01491J
- [52] Yim WM, Paff RJ. Thermal expansion of AlN, sapphire, and silicon. *Journal of Applied Physics*. 1974;**45**:1456-1457

[53] Wu C, Wang J, Chan MH, Chen TT, Gwo S. Heteroepitaxy of GaN on Si(111) realized with a coincident-interface AlN/ $\beta$ -Si<sub>3</sub>N<sub>4</sub>(0001) double-buffer structure. *Applied Physics Letters*. 2003;**83**:4530-4532

[54] Bourret A, Barski A, Rouviere JL, Renaud G, Barbier A. Growth of aluminum nitride on (111) silicon: Microstructure and interface structure. *Applied Physics Letters*. 1998;**83**:2003-2009

[55] Şahin H, Cahangirov S, Topsakal M, Bekaroglu E, Akturk E, Senger RT, et al. Monolayer honeycomb structures of group-IV elements and III-V binary compounds: First-principles calculations. *Physical Review B*. 2009;**80**:155453

[56] Mukhopadhyay G, Behera H. Structural and Electronic Properties of Graphene and Graphene-like Materials. 2012. Available from: <http://arxiv.org/abs/1210.3308>

[57] Tsipas P, Kassavetis S, Tsoutsou D, Xenogiannopoulou E, Golias E, Giamini SA, et al. Evidence for graphite-like hexagonal AlN nanosheets epitaxially grown on single crystal Ag(111). *Applied Physics Letters*. 2013;**103**:251605

[58] Freeman CL, Claeysens F, Allan NL, Harding JH. Graphitic nanofilms as precursors to Wurtzite films: Theory. *Physical Review Letters*. 2006;**96**:066102

[59] Tusche C, Meyerheim HL, Kirschner J. Observation of depolarized ZnO (0001) monolayers: Formation of unreconstructed planar sheets. *Physical Review Letters*. 2007;**99**:026102